Visuomotor Reinforcement Learning for Multirobot Cooperative Navigation

Zhe Liu, Qiming Liu, Ling Tang, Kefan Jin, Hongye Wang, Ming Liu, *Senior Member, IEEE*, and Hesheng Wang, *Senior Member, IEEE*

***Abstract*— This article investigates the multirobot cooperative navigation problem based on raw visual observations. A fully end-to-end learning framework is presented, which leverages graph neural networks to learn local motion coordination and utilizes deep reinforcement learning to generate visuomotor policy that enables each robot to move to its goal without the need of environment map and global positioning information. Experimental results show that, with a few tens of robots, our approach achieves comparable performance with the state-of-the-art imitation learning-based approaches with bird-view state inputs. We also illustrate our generalizability to crowded and large environments and our scalability to ten times number of the training robots. In addition, we demonstrate that our model trained for multirobot case can also improve the success rate in the single-robot navigation task in unseen environments.**

***Note to Practitioners*—With the development of intelligent industrial and logistic systems, robotic transportation systems are widely implemented. However, existing multirobot path coordination and navigation approaches are basically under some unreasonable assumptions, which are very hard to be implemented in practical scenarios. This article aims to greatly promote the real application of learning-based multirobot cooperative navigation approach, in order to achieve the following. First, we introduce an end-to-end reinforcement learning framework instead of the commonly used imitation learning strategy, as the latter one needs exhaustive training data to cover all the scenarios and does not have the required generalizability. Second, we directly use the raw sensor data instead of the commonly used bird-eye-view semantic observations, as the latter one is generally not representative of practical application scenario from the robot perspective and cannot solve the occlusion issue. Third, we interpret our learned model to illustrate which parts of the input and shared observations contribute most to the robots' final actions. The above interpretability ensures predictability (thus safety) of our visuomotor policy in practical applications. Our learned visuomotor policy has the ability to coordinate dozens of robots by only using raw visual observations in unknown environments without map nor global localization information, this is the first time in the literature. Our future work includes solving the sim-to-real issue and conducting physical experiments.**

***Index Terms*— Cooperative navigation, multirobot system, reinforcement learning (RL), visuomotor.**

I. Introduction

MULTIROBOT cooperative navigation, which requires each robot to navigate to its goal position autonomously while ensuring motion coordination (i.e., collision avoidance) with other robots, is of great importance in several application scenarios, such as multirobot cooperative transportation [1], multiagent navigation [2], [3], drone and robot swarm formation control [4], [5], and multivehicle platoon control [6], [7]. Traditional approaches include the centralized approach [8], decentralized approach [9], and hierarchical approach [10]. Centralized approach aims at finding out the optimal multirobot spatiotemporal trajectories with as lower computational complexity as possible, and however, it can only be used in a deterministic environment and its scalability to large-scale problems cannot be ensured [10]. The decentralized approach utilizes local traffic rules or motion coordination strategies to achieve flexibility in robot scales, and however, it cannot handle the local crowded space and generalizes poorly to various environments [11]. In order to combine the advantages of the above two categories, the hierarchical approach introduces a high-level planner to optimize overall system performance and utilizes local motion coordination to ensure safety. However, their high computational complexity and the requirement of high-frequency global information storage/retrieval greatly limit their applications.

More recently, learning-based approaches have been investigated to solve the multirobot cooperative navigation problem,

Manuscript received June 25, 2021; accepted August 24, 2021. This article was recommended for publication by Associate Editor T. Xu and Editor D. O. Popa upon evaluation of the reviewers' comments. This work was supported in part by the Natural Science Foundation of China under Grant 62073222 and Grant U1913204, in part by Shanghai Municipal Education Commission and Shanghai Education Development Foundation through "Shu Guang" Project under Grant 19SG08, in part by Shenzhen Science and Technology Program under Grant JSGG20201103094400002, and in part by the Science and Technology Commission of Shanghai Municipality under Grant 21511101900. *(Zhe Liu and Qiming Liu contributed equally to this work.) (Corresponding author: Hesheng Wang.)*

Zhe Liu is with the Department of Computer Science and Technology, University of Cambridge, Cambridge CB2 1TN, U.K. (e-mail: zl457@cam.ac.uk).

Qiming Liu, Ling Tang, and Hongye Wang are with the Department of Automation, Shanghai Jiao Tong University, Shanghai 200240, China (e-mail: qimingliu@sjtu.edu.cn; elftat@sjtu.edu.cn; wanghongye@sjtu.edu.cn).

Kefan Jin is with the MOE Key Laboratory of Marine Intelligent Equipment and System and the State Key Laboratory of Ocean Engineering, Shanghai Jiao Tong University, Shanghai 200240, China (e-mail: jinkefan@sjtu.edu.cn).

Ming Liu is with the Department of Electronic and Computer Engineering, The Hong Kong University of Science and Technology, Hong Kong (e-mail: eelium@ust.hk).

Hesheng Wang is with the Department of Automation, Key Laboratory of System Control and Information Processing of Ministry of Education, Key Laboratory of Marine Intelligent Equipment and System of Ministry of Education, Shanghai Engineering Research Center of Intelligent Control and Management, Shanghai Jiao Tong University, Shanghai 200240, China (e-mail: wanghesheng@sjtu.edu.cn).

Color versions of one or more figures in this article are available at https://doi.org/10.1109/TASE.2021.3114327.

Digital Object Identifier 10.1109/TASE.2021.3114327

which learns fully distributed local action policies by aggregating local observations and shared information from neighboring robots [3], [12], [13]. Learning-based approaches have achieved promising performances, especially under system uncertainties and dynamics. However, current models are trained on datasets that assume complete state observability of the local environment from the bird-eye view. These are generally not representative of real-world application scenario from the robot perspective and cannot be achieved when onboard sensors are occluded. In addition, they have implicitly divided the raw perception, state estimation (bird-view state observation), and navigation policy learning into separate functional modules, which prohibits any potentially direct feedback between the raw sensor data and the final navigation policy and also cannot be learned in a fully end-to-end manner in practical implementations.

In this article, we utilize the first-person-view raw observations as system input and learn visuomotor policy for multirobot cooperative navigation tasks in unknown environments. Our main contributions can be summarized as follows.

1) To the best of the authors' knowledge, this article builds the first reinforcement learning (RL) framework for the multirobot cooperative navigation task with first-person-view visual data. The proposed system is fully distributed and only local observations are required, i.e., each robot does not need the environment map nor any global location information. These move a big step to achieve the real implementation in practical applications.
2) A fully end-to-end learning framework is presented to bridge the semantic gap from the raw perception data to the end decision-making. First, deep learning techniques are utilized to extract high-dimensional features from raw visual observations and compact them into efficient representations. Second, graph neural networks (GNNs) are implemented to learn information sharing and aggregation among neighboring robots for efficient local motion coordination. Third, the RL strategy is implemented to generate a proper visuomotor policy for robot control. In contrast to imitation learning (IL)-based works, our approach does not need exhaustive expert data and scales well to unseen scenarios.
3) Comprehensive validation results show that, for a few tens of robots, our RL-based visuomotor policy achieves a comparable performance with the state-of-the-art IL approaches with bird-view state observations. We demonstrate our scalability to large-scale robot networks (ten times number of the training robots) and crowded and large environments (25 times crowdedness of the training case). In addition, we demonstrate that our multirobot visuomotor training can also benefit the single-robot RL navigation ability in unknown environments.

II. Background and Related Work

A. Traditional Approaches

As mentioned above, traditional multirobot cooperative navigation approaches can be classified into centralized, decentralized, and hierarchical approaches. Centralized approaches, represented by the conflict-based search (CBS) [8], ensure completeness and optimality under some certain metrics such as makespan or flowtime [8]. The main shortage of these approaches is that they assume that the deterministic environment, dynamics, and uncertainties in the execution stage will greatly degrade the actual robot navigation performance [10]. Decentralized approaches, represented by the priority-based [14] and time-window-based [15] approaches, introduce motion priority, local traffic rule, or velocity coordination mechanism [9] to solve local conflicts. Decentralized approaches scale well to large robot groups, and however, due to their incompleteness and the need of predefined strategies, their performance declines in crowded local spaces and generalizes poorly to various scenarios [11]. Hierarchical approaches, represented in [10], [16], optimize system-level performance such as the traffic flow and working throughput in a centralized manner and coordinate robots' spatiotemporal trajectories locally, thus improving the optimality and scalability simultaneously. However, as a centralized information-sharing system is required for high-level scheduling and multiple decentralized local planning centers are typically implemented for coordination [10], both the high system synchronization requirements and the frequent global information storage/retrieval need greatly limit their applications.

B. Learning-Based Approaches

Pioneered by PRIMAL [3], both the IL and RL approaches have been studied for solving the multirobot navigation and motion coordination problems [11]–[13], [17]. Basically, compared to RL-based works, IL-based approaches have advanced successful rate and scale well to hundreds or even thousands of robots [3], [13]. However, they rely on supervised learning with expert planners and exhaustive data that are hard to be obtained, especially to cover all the unexpected scenarios. In order to let the model to explore more potential solutions, RL-based approaches become more and more popular in most recent days, which have better generalizability and are more adaptive to various environments [18]. However, RL-based approaches commonly suffer from the reward sparsity and sample in-efficiency issues, especially in the initial training stage. Almost all the existing learning-based approaches assume complete observability of the local environment and input the abstract state observation from the bird-eye view. These are typically not representative of real-world scenarios from the robot's own perspective. In addition, in order to achieve this, they need to divide the raw perception, state estimation, and navigation policy learning into separate functional submodules with several preprocessing operations and introduce hand-tuned parameters. In this article, we directly utilize raw visual sensor data as the network input and implement a fully end-to-end framework to learn visuomotor policy.

C. Visuomotor Learning for Robot Navigation

Visuomotor policy learning has been investigated for drone navigation [19], mobile manipulation [20], and self-driving

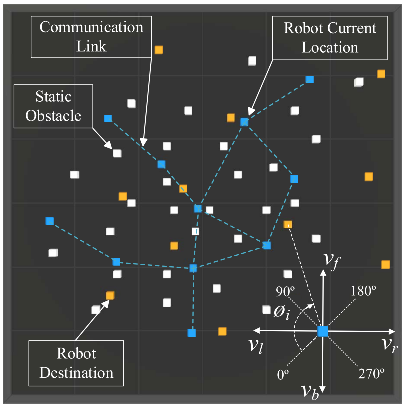

(a)

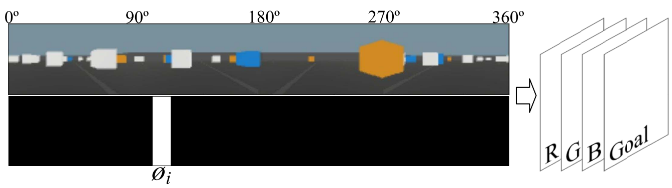

(b)

Fig. 1. System formulation of the visuomotor learning for multirobot cooperative navigation. (a) Multirobot cooperative navigation system and the coordinates system definition. (b) Input observation of each robot, where we transfer the goal direction information into a virtual image and then concatenate it with the omnidirectional RGB image to form the multichannel input observation.

applications [21] for several years. In order to efficient feature representation learning, autoencoders [19] and auxiliary tasks [21] are commonly used. Goal information can be introduced by 2-D global map [22], target images [23], or relative distances to several scenario landmarkers [21]. In addition, progressive net [24] and adversarial approach [20] can be further utilized to achieve sim2real domain transfer. Note that all the above works focus on the single-robot case. For a multirobot case, a vision-based drone formation control approach is presented in [4], which uses a behavior-based flocking controller as the expert to train the vision-based control policy. This method can only imitate the expert controller to achieve some simple swarm behaviors in obstacle-free spaces. Similarly, Hu *et al.* [25] provided a vision-based perception network to learn the required state estimation, which is not end-to-end and also needs an expert dataset for supervised learning. To sum up, end-to-end visuomotor learning for multirobot cooperative navigation in unknown environments is still an open challenge.

III. Problem Formulation and System Design

In this article, we consider the 3-D continuous environment space $\mathcal{W} \subseteq \mathbb{R}^3$, which contains a set of N_s static obstacles $\mathcal{S} = \{s_1, \ldots, s_{N_s}\}$ randomly located on the ground. As shown in Fig. 1, a set of N_r mobile robots $\mathcal{R} = \{r_1, \ldots, r_{N_r}\}$ navigate on the ground plane of the free space $\mathcal{W} \setminus \mathcal{S}$. The robot goal positions $\mathcal{G} = \{g_1, \ldots, g_{N_r}\}$ are also randomly located on the ground plane of the free space $\mathcal{W} \setminus \mathcal{S}$. Let $p_i(t)$ denote the position of r_i at time step t, and the objective of the multirobot cooperative navigation can be defined as: for a maximum time step t_m, $\forall i$, $p_i(t_m) = g_i$, and $\forall i, j, t$, we require $p_i(t), p_j(t) \subset \mathcal{W} \setminus \mathcal{S}$ and $p_i(t) \neq p_j(t)$, i.e., each robot r_i should reach its goal position g_i without any collisions with static obstacles or other robots.

In our system formulation, we make the following assumptions. First, each robot r_i can communicate with its neighbors $r_j \in \mathcal{N}_i(t) = \{r_j | D(p_i(t), p_j(t)) < C_r\}$, where $D(\cdot,\cdot)$ represents the Euclidean distance and C_r is the communication range. Second, we do not consider additional dynamic obstacles except for the moving robots in the environment. Third, each robot can obtain rough direction information of its goal during movements. Please note that here, we do not assume the specific coordinates (exact location) of the goal relative to the robot. In addition, except for this direction information, we do not need any other global location nor relative distance information of the goal and neighboring robots, also we do not need the global environment map. This aims to ensure the implementation of our multirobot cooperative navigation approach in any unseen environments. Fourth, the robots have no orientation and their visual observations are omnidirectional, and the coordinate system of each robot is defined in the bottom right of Fig. 1(a). The omnidirectional observation and movement assumptions aim to facilitate each robot to learn the relative positioning information of the communicated neighbors as well as their motion intentions. Note that this assumption can be easily alleviated in practical implementations by using the "rotate-move-rotate" strategy in each moving step of each robot, and only a compress sensor is required.

As shown in Fig. 1(b), at each time step t, each robot r_i obtains the local observation O_t^i, which contains four input channels, the first three channels are the omnidirectional RGB image of its surrounding environment with the size of 384×54, and the last channel is a virtual image with the same size that contains the goal direction information. Similar to the omnidirectional image, the leftmost and rightmost columns in the goal channel correspond to 0^o and 360^o in the coordinates system defined in Fig. 1(a), and then, the column (with a width of 20) corresponded to the goal direction ϕ_i is highlighted with the white color and all the other columns are with the black color.

We consider the velocity control of the robot in the continuous environment space. As shown in Fig. 1(a), the robot action set is defined as $\mathcal{A} = \{v_f, v_b, v_l, v_r, v_\emptyset\}$, i.e., at each time step t, each robot can move front, back, left, or right with a constant velocity or stay in its current location.

Based on the above formulations, we now build our multirobot cooperative navigation framework. For each robot, our end-to-end learning framework includes three main modules as follows.

1) *Observation Feature Learning:* As shown in Fig. 2, the input tensor of each robot's network is a time series of the multichannel observations $\{O_t^i, O_{t-1}^i, \ldots, O_{t-N_t}^i\}$. Then, we utilize a series of convolution layers followed by a fully connected (FC) layer to extract

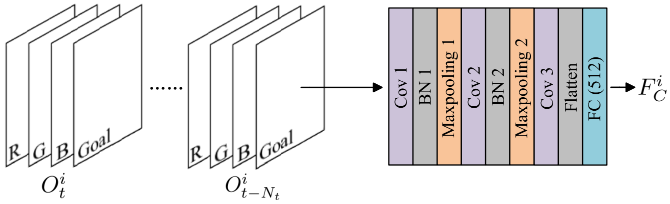

Fig. 2. Network structure of the observation feature learning module, where we input time series observations and utilize convolution layers to extract high-dimensional features for the input observation of each robot. Cov: convolution layer. BN: batch normalization. FC: fully connected layer.

high-dimensional features F_C^i from the input tensor. For simplification, we remove the time dimension t here.

2) *Local Coordination Information Learning:* Inspired by [13], [25], we share the learned observation features among neighboring robots and introduce GNN layers to aggregate the shared messages for learning the local coordination information. For each robot r_i, a high-dimensional coordination feature F_G^i is obtained by aggregating the visual observation as well as motion intention of local neighbors.

3) *Visuomotor Policy Learning:* Finally, we concatenate F_G^i and F_C^i to form the input of visuomotor policy learning module and use a series of FC layers to estimate the value function and the quality of each state–action pair. The action with the best quality will be chosen with the highest probability.

Our main principle in the above system design is to keep our network structure as parameter economic as possible, in order to make the network easy training and ensure the real-time performance. Please note that, if necessary, one can always introduce more complex network structures in each of the above three modules to further improve model capacity and performance.

In the following, we will describe our coordination information learning and visuomotor policy learning modules.

IV. Local Coordination Information Learning

In order to achieve cooperative navigation, the learned observation feature of each robot can be shared locally among neighboring robots. Sharing the observation features helps the robots to learn their relative positions and enables the robots to extend perception range by fusing neighbors' observation features. In addition, as the goal direction information is also contained in the observation features, each robot can also obtain the moving intentions of its neighbors, thus facilitating the learning of local motion coordination and conflict avoidance. In this article, we introduce the GNN module to achieve the above local coordination information learning.

We first define $\Psi_d = \{\psi_d^{ij}\} \in \mathbb{R}^{N_r \times N_r}$ as the adjacency matrix, which describes the neighboring relations, i.e., if robot $r_j \in \mathcal{N}_i(t)$, then $\psi_d^{ij} = \psi_d^{ji} = 1$; otherwise, $\psi_d^{ij} = 0$ (here, the subscript d represents the direct communication). In our preliminary testings, we find that only aggregating the information from the direct neighbors is not adequate for local motion coordination, as each robot should consider the motion intentions of more distant robots in advance to plan its future motions and avoid potential future collisions. Fortunately, through multihop routing [26] or multiround information sharing [13], each robot can obtain its multi-hop neighbors' information while still maintaining the fully distributed framework. In order to balance the complexity and performance, we consider two-hop neighbors' information in local coordination information learning. We define $\Psi_e = \{\psi_e^{ij}\} \in \mathbb{R}^{N_r \times N_r}$ is the adjacency matrix of the extended communication graph, i.e., for three robots r_i, r_j and r_k, if $r_i \in \mathcal{N}_k(t)$ and $r_j \in \mathcal{N}_k(t)$ simultaneously but $r_j \notin \mathcal{N}_i(t)$, then $\psi_e^{ij} = \psi_e^{ji} = 1$, otherwise $\psi_e^{ij} = 0$. We further define $\tilde{\Psi}_d = \{\tilde{\psi}_d^{ij}\} = \Psi_d + I_{N_r}$, $\tilde{\Psi}_e = \{\tilde{\psi}_e^{ij}\} = \Psi_e + I_{N_r}$, which introduce the self-loop information.

As shown in Fig. 3, the local coordination information learning module inputs each robot's observation features F_C^i extracted by the observation feature learning module and two GNN layers are implemented to aggregate neighbors' features. More specifically, the input feature matrix of the first GNN layer is $H^{(0)} = [F_C^1, \ldots, F_C^{N_r}]^T$, where the ith row is the feature vector of the robot r_i. The output of the first GNN layer is

$$H^{(1)} = \left[\sigma\left(\mathbb{F}_d\left(H^{(0)}, \tilde{\Psi}_d, W_d^{(1)}\right)\right), \sigma\left(\mathbb{F}_e\left(H^{(0)}, \tilde{\Psi}_e, W_e^{(1)}\right)\right)\right] \quad (1)$$

where $\mathbb{F}_d(\cdot,\cdot,\cdot)$ and $\mathbb{F}_e(\cdot,\cdot,\cdot)$ represent the graph convolution operation on the direct communication graph $\tilde{\Psi}_d$ and extended communication graph $\tilde{\Psi}_e$, respectively, $W_d^{(1)}$ and $W_e^{(1)}$ represent learnable weight matrices, and $\sigma(\cdot)$ represents the elementwise nonlinear activation function. Then, we introduce the second GNN layer to fully exploit the feature aggregation and extraction ability of GNN and the final output of the local coordination information learning module is

$$\begin{aligned} H^{(2)} &= \left[\sigma\left(\mathbb{F}_d\left(H^{(1)}, \tilde{\Psi}_d, W_d^{(2)}\right)\right), \sigma\left(\mathbb{F}_e\left(H^{(1)}, \tilde{\Psi}_e, W_e^{(2)}\right)\right)\right] \\ &= \left[F_G^1; F_G^2; \ldots; F_G^{N_r}\right] \end{aligned} \quad (2)$$

where F_G^i represents the feature vector of robot r_i.

In this article, we utilize the following two kinds of GNN to formulate the graph convolution operation $\mathbb{F}_\circ(H^*, \tilde{\Psi}_\circ, W_\circ^\star)$ in each graph convolution layer (where $\circ$ can be $_e$ or $_d$, $*$ can be $^{(0)}$ or $^{(1)}$, and $\star$ can be $^{(1)}$ or $^{(2)}$).

1) *Graph Convolution Network (GCN):* Define the diagonal degree matrix $\tilde{M}_\circ = \{\tilde{m}_\circ^{ii}\} \in \mathbb{R}^{N_r \times N_r}$ where $\tilde{m}_\circ^{ii} = \sum_j \tilde{\psi}_\circ^{ij}$, and then, GCN has the following formulation:

$$\mathbb{F}_\circ(H^*, \tilde{\Psi}_\circ, W_\circ^\star) = \tilde{M}_\circ^{-\frac{1}{2}} \tilde{\Psi}_\circ \tilde{M}_\circ^{-\frac{1}{2}} H^* W_\circ^\star. \quad (3)$$

Normalizing the adjacency matrix by using the diagonal degree matrix contributes to unify the scale of each robot's feature vector. The above GCN is based on the graph Fourier transform theory and is well simplified by using the first-order Chebyshev polynomial approximation, which can prevent the gradient vanishing or exploding problem.

2) *Graph Attention Network (GAT):* We compute a convolution similar to GCN introduced above but use the attention mechanism [27] to weight the adjacency matrix instead of using the normalized adjacency matrix

$$\mathbb{F}_\circ(H^*, \tilde{\Psi}_\circ, W_\circ^\star) = \alpha_\circ^\star H^* W_\circ^\star + b_\circ^\star \quad (4)$$

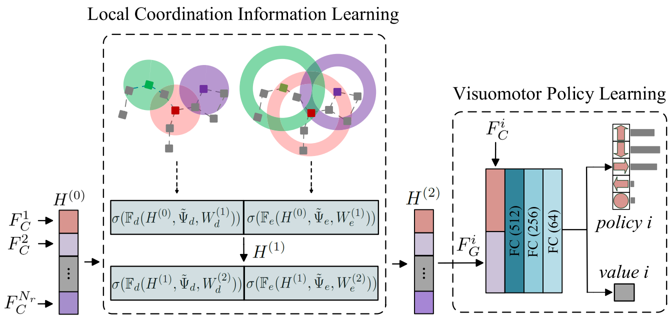

Fig. 3. Network structures of the neighbor information aggregation and control policy generation modules. In the neighbor information aggregation module, graph convolution operation is conducted on different hop neighbor sets and multilayer graph aggregation is introduced. In the control policy generation module, a series of FC layers is used to learn action policy with RL strategy.

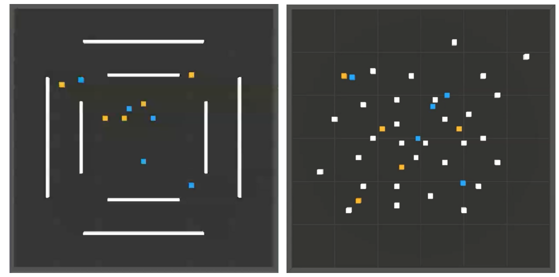

(a) (b)

Fig. 4. Training environments for curriculum learning, where a simple structured environment is considered in the first stage and a more complex environment is considered in the second stage. Similar to Fig. 1, the blue and yellow blocks represent the current and goal location of each robot, and the white blocks represent static obstacles. (a) Simple environment. (b) Clutter environment.

where $b_\circ^\star$ is the trainable bias and

$$\{\alpha_\circ^\star\}_{ij} = \frac{\exp\left(\mathrm{LR}\left(\mathbf{a}^T\left[\left(H^* W_\circ^\star\right)_i, \left(H^* W_\circ^\star\right)_j\right]\right)\right)}{\sum_{\tilde{\psi}_\circ^{ik}=1} \exp\left(\mathrm{LR}\left(\mathbf{a}^T\left[\left(H^* W_\circ^\star\right)_i, \left(H^* W_\circ^\star\right)_k\right]\right)\right)}. \tag{5}$$

LR represents the *LeakyReLU* activation function, $\mathbf{a} \in \mathbb{R}^{2\ N_r}$ is a trainable attention kernel, and $(X)_i$ represents the ith row in X.

V. Visuomotor Policy Learning

Based on the observation features and coordination information learned above, in this section, we describe our visuomotor policy learning approach for cooperative navigation.

A. Visuomotor RL

As shown in Fig. 3, we concatenate the output feature vectors of the observation feature learning module and local coordination information learning module, i.e., F_C^i and F_G^i, and use a series of FC layers to build the visuomotor policy network, which generates robot action a_t^i. Concatenating F_C^i and F_G^i aims to integrate each robot's own visual observation and goal information and also the neighbors' observation and moving intentions, thus helping the robot to navigate to its goal while coordinating motions with others.

In this article, we use the RL strategy for visuomotor policy learning. The reward function Υ_t^i of each robot is defined as follows.

1) A small negative step reward $\Upsilon_t^i = -(\gamma_1/N_m) < 0$ to drive the robot to reach the goal as soon as possible, where N_m is the maximum moving step;
2) An extra-large negative reward $-\gamma_2$ if the robot collides with other robots or static obstacles, i.e., $\Upsilon_t^i = -(\gamma_1/N_m) - \gamma_2 < 0$.
3) An extra positive reward (γ_3/N_m) if the robot's action aligns to the optimal path from its current position to its goal, then $\Upsilon_t^i = (\gamma_3 - \gamma_1/N_m) > 0$. In each step, we calculate the optimal path and compare the robot action direction with the first step on the optimal path, if they are aligned (choosing the same moving direction from the four directions in $\mathcal{A}$), and we give the extra positive reward (γ_3/N_m).
4) An extra-large positive reward γ_4 if the robot arrives its goal, i.e., $\Upsilon_t^i = -(\gamma_1/N_m) + \gamma_4 > 0$.

The optimal path can be calculated by using the Dijstra or A* method. An implementation problem is that we consider continuous environment space in this article, and however, the optimal path does need to be carried out in the discrete environment with topology graphs. In order to address this issue, we temporally discretize the free space $\mathcal{W} \setminus \mathcal{S}$ to obtain a grid topology map and the discretization step is set to one unit length. During training, the current and target position of each robot will be approximated to the nearest nodes in the discretized map, based on which the optimal path will be generated. Introducing the optimal path information aims to provide each robot a dense reward at each step. Please note that the optimal path information is only used in the training. In addition, in order to decrease the computational complexity, an event-triggered strategy is introduced, i.e., we only update the optimal path when the robot's position in the discretized map changes in this time step.

B. Curriculum Learning Strategy

Although we provide a dense reward function for each robot, the model training of multirobot cooperative navigation is still very challenging, as we build a fully end-to-end RL framework with raw visual inputs. In this article, we utilize the curriculum learning strategy to increase sample efficiency and accelerate the training speed. More specifically, we first train our model in a simple and structured environment [as shown in Fig. 4(a)] and then transfer the trained network to a more complex and clutter environment [as shown in Fig. 4(b)] for further training. Both of the environments are with the size of 60×60 and contain five robots. The obstacle density in the second environment is about 1%.

We first use the simple and structured environment shown in Fig. 4(a), and the robots' initial and goal positions are generated more frequently in the open area located at the center of the environment so that robots can learn the visual characteristics of the goal more easily during the early training

TABLE I
NETWORK STRUCTURE OF THE OBSERVATION FEATURE LEARNING MODULE

	kernel size	stride	channel number
Cov1	(3,5)	(1,3)	16
Maxpool1	(2,2)	(1,1)	
Cov2	(4,4)	(2,2)	32
Maxpool2	(2,2)	(1,1)	
Cov3	(4,4)	(2,2)	64

TABLE II
COMPUTATIONAL COMPLEXITY OF EACH BASELINE MODEL

	Parameters	Runtime per step
SRV	14,086,896	31.279ms
MRV-C $\backslash w.$ *SC*	14,611,184	32.796ms
MRV-A $\backslash w.$ *SC*	14,614,256	34.212ms
MRV-C	14,873,328	33.154ms
MRV-A	14,875,376	34.770ms

stage. At the same time, a few robots' goal positions will also appear behind the obstacles, which allows the robots to have some basic obstacle-avoidance capabilities. The first stage training will automatically stop when the following conditions are met.

1) Reward curve is stable (evaluated by its variance) for more than 100 thousand steps.
2) Average episode reward is above N_e for more than 100 thousand steps.
3) The average number of collisions in the past five rounds is less than N_c for each robot.

We then transform the trained model into a complex and crowded environment, as shown in Fig. 4(b). The robot cannot always see its goal directly at the initial position, and the distance from the robot's initial location to the goal is also enlarged. Due to the preliminary navigation and obstacle-avoidance capabilities learned in the previous stage, the robots can navigate to their goal location in the complex environment, but with an unskilled manner (large detours). The second stage of training can further strengthen the robots' navigation and obstacle-avoidance abilities and shorten the time of goal searching in the complex environment.

VI. IMPLEMENTATION

A. Model Parameters

We use proximal policy optimization [28] as the RL algorithm in our implementation, which is an actor–critic method based on a combination of policy and value gradient. The default parameters are set as follows: the reward parameters $\gamma_1 = 10$, $\gamma_2 = 1$, $\gamma_3 = 20$, $\gamma_4 = 10$, $N_e = 20$, $N_c = 3$, and $N_m = 400$. The observation feature learning module is described in Table I followed with a flatten operation and an FC layer with 512 unit. The activation functions are `ReLU`. For the local coordination information learning module, $F_C^i \in \mathbb{R}^{512}$, $F_G^i \in \mathbb{R}^{512}$, $H^{(0)}, H^{(1)}, H^{(2)} \in \mathbb{R}^{N_r \times 512}$, $W_d^{(1)}, W_d^{(2)} \in \mathbb{R}^{512\times 256}$, and $W_e^{(1)}, W_e^{(2)} \in \mathbb{R}^{512\times 256}$. In the visuomotor policy learning module, we use three FC layers with 512, 256, and 64 units, respectively.

B. Training and Testing

We train our model with Intel i7-8700K CPU and one NVIDIA GTX 1080Ti GPU, Python 3.7 with TensorFlow 2.3. The initial learning rate is 4×10^{-5} and will linearly decay to 4×10^{-6} in one million steps. The training optimizer is `Adam`. We use curriculum learning strategy to help robots converge to a reasonable strategy faster, which has been explained in detail in Section V-B. During the training process, episode switching conditions include: 1) all agents reach there own goal and 2) simulation step of current episode reaches a maximum number defined as 300, which is smaller than maximum simulation steps N_m in testing, as we expect the robot to collect more representative data and filter out invalid and failed cases during training. If one of the above conditions is satisfied, we will end the current episode and start a new one. In training, the static obstacles in the environments shown in Fig. 4 are fixed in different episodes, but the robots' initial and goal locations are changed.

We introduce a different number of robots (1, 5, 10, 30, and 50), static obstacle densities (4%, 8%, and 12%), and environment sizes (40 × 40, 60 × 60, and 100 × 100) to build the various of testing environments. We will comprehensively test the generalizability and scalability of different model structures in different environments, which will be introduced in detail in the following. The following metrics are used for performance evaluation.

1) *Success Rate:* As mentioned before, we set a maximum step $N_m = 400$ for all the tests and count the number N_{ra} of the robots that reach their goal within this time. Then, we calculate the successful rate (N_{ra}/N_r) of each evaluation.
2) *Path Length:*
$$\text{Path Length} = \frac{1}{N_{\text{ra}}} \sum_{i=1}^{N_{\text{ra}}} \frac{\mathcal{L}_i}{\mathcal{L}_{\text{opt}}^i} \quad (6)$$
where $\mathcal{L}_i$ is the actual moving distance of each robot r_i and $\mathcal{L}_{\text{opt}}^i$ is the length of the optimal path between the robot's initial position and goal, which is defined in Section V-A. Please note that in the multirobot path planing case, the shortest path $\mathcal{L}_{\text{opt}}^i$ typically cannot be achieved, even for the optimal solution, each robot should also take a detour or temporarily stop for locally coordinating its motion with other robots.
3) *Moving Step:* This measure corresponds to the average moving steps of the robots that arrive their goal successfully. For those robots which cannot reach their goal, we use the maximum time step N_m.

C. Baseline Models

In the results, we consider the following five different network structures and compare their performance for ablation study.

1) *MRV-C:* This is our complete model, which utilizes GCN described in Section IV for the local coordination information learning module. Here, MRV represents multirobot visual-based cooperative navigation and *C* represents GCN.
2) *MRV-A:* This is our complete model, which utilizes GAT described in Section IV for the local coordination information learning module. Here, *A* represents GAT.
3) *MRV-C $\backslash w$. SC:* In this model, we utilize GCN in the local coordination information learning module and directly input the learned feature vector F_G^i to the visuomotor policy learning module (do not concatenate F_G^i with the observation feature F_C^i). Here, $\backslash w$. *SC* represents "without the skip connection of the observation feature F_C^i."
4) *MRV-A $\backslash w$. SC:* In this model, we utilize GAT in the local coordination information learning module and directly input the learned feature vector F_G^i to the visuomotor policy learning module without concatenating the observation feature F_C^i."
5) *SRV:* In this model, each robot independently learns its visuomotor policy without communicating with others (treats other robots as noncommunicative dynamic obstacles), i.e., we directly input the observation feature vector F_C^i to the visuomotor policy learning module. Here, SRV represents the single-robot visual navigation.

In Table II, we show the number of parameters and the real runtime per step of each baseline model mentioned above. The results show that most of the parameters (and also the spent computation time) are in the observation feature learning module. This implies that introducing the local coordination feature learning module does not largely increase the storage and computation complexity, and however, as will be shown in Section VII, it will largely improve the performance.

VII. RESULTS

In this section, we conduct comprehensive validations and comparisons to demonstrate the effectiveness, generalizability, and scalability of our approach. All the validations are conducted in Unity using ML-Agents toolkit [29].

A. Convergence Performance in Training

As mentioned in Section V-B, we introduce the curriculum learning strategy to increase the sample efficiency, especially in the initial training period. The cumulative reward of each episode in each training stage is shown in Fig. 5(a), where the dotted line indicates the actual switch time in the training of each model. The average moving step of each model in each episode is shown in Fig. 5(b). Please note that in training, we set the time-out moving step as 300 and will terminate this iteration at this time if any robot cannot reach its goal within 300 steps.

The training curves in Fig. 5 show that the following conditions hold.

1) Introducing the skip connection (i.e., the concatenation of F_C^i and F_G^i) in the input of the visuomotor policy learning module greatly improves the convergence speed in the first training stage. In the presence of skip connection, the GNN module can only focus on the efficient feature sharing and aggregation task, while it does not need to simultaneously learn to integrate the visual features extracted by the observation feature learning module. Fig. 5(a) shows that `MRV-A \w. SC` even cannot converge in the first training stage, which results from the great challenges of learning the perception, attention policy, information aggregation, and visuomotor control modules simultaneously. Please note that each robot does not know what its goal looks like (in our simulator, the goal of all the robots looks the same) and it can only be learned after the robot receives the responding reward, and this also increases the difficulty of the initial learning stage.
2) `SRV`, `MRV-C`, and `MRV-A` converge quickly in the initial stage. The introduced goal direction information and the proposed dense reward help to increase the sample efficiency during the initial training stages.
3) The switch times of `MRV-C` and `MRV-A` are earlier than that of `SRV`. In addition, `MRV-C` performs better than `MRV-A` as the latter one has more learnable parameters.
4) `SRV` has the best performance only in the very early training stage, and the potential reason is that it has less learnable parameters and obtains more rewards in simple tasks in the initial training stage. However, as it is very hard for `SRV` to learn the motion coordination ability, its overall convergence speed is slower than `MRV-C` and `MRV-A`.

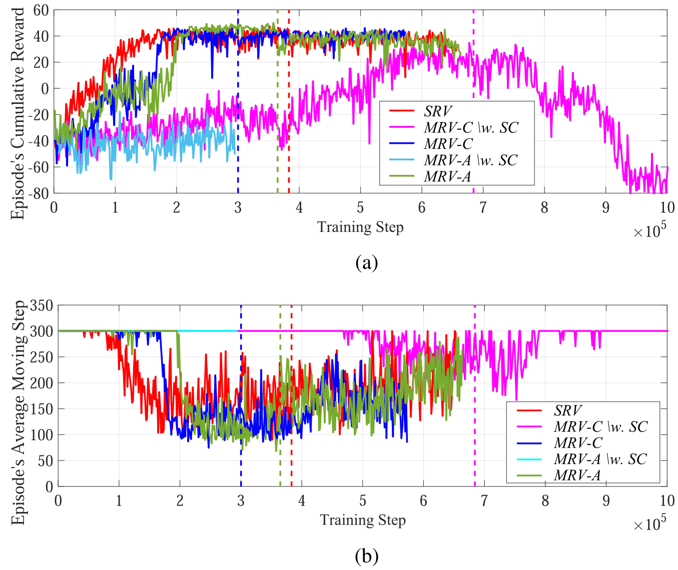

Fig. 5. Training performance of different baseline models. (a) Cumulative reward in each episode. (b) Average moving step in each episode.

B. Evaluation Results

In this section, we test different networks on testing environments that have the same map size and robot number with the training environments, but the testing environments have a larger obstacle density (about 4%). The results in Table III

TABLE III
COMPARISON RESULTS OF DIFFERENT NETWORKS

	Success Rate	Path Length	Moving Step
SRV	88.40%(14.10%)	1.38(0.55)	137.45(72.05)
MRV-C $\backslash w.$ *SC*	93.33%(10.75%)	1.49(0.58)	133.88(66.97)
MRV-C	**95.87%(9.32%)**	1.39(0.52)	133.55(68.69)
MRV-A	95.60%(9.20%)	**1.32(0.52)**	**115.41(69.96)**

In each item, we provide the average value and the standard deviation among 150 repeated tests. The bold values perform best.

show that the following conditions hold. First, both the success rates of `MRV-C` and `MRV-A` are higher than 95%, which are similar to the results obtained by the state-of-the-art imitation learning-based approach [13]. Note that we directly input the first-person-view visual observations and do not need an expert dataset for supervised learning, and thus, our approach is more promising in real applications. Second, `MRV-A` performs better than `MRV-C` since it has a very similar success rate but much lower path length and moving step.

C. Scalability to Large-Scale Robot Networks

In this section, we directly use different models trained with five robots to test their scalability to large-scale problems with 10, 30, and 50 robots. The testing environments have the same map size (60 × 60) with the training maps but have a larger obstacle density (about 4%). Combining the results in Tables III and IV, we can find that the following conditions hold.

1) By introducing the GNN with skip connection, success rate can be largely improved in all the cases. Even for the 50 robots case (ten times the training robot number), `MRV-C` still has about 78% success rate. In addition, the performance degradation of `MRV-C` and `MRV-A` in large-scale problems is also lower than `SRV`.
2) The performance of `MRV-C \w. SC` declines largely with the increasing robot number and is even much worse than `SRV`. This indicates that, without skip connection, the model cannot learn how to efficiently aggregate the self-observation features and the shared messages from others. In large-scale problems, each robot receives a large number of shared messages, which will dilute the perception signal of the robot itself, so without an independent perception signal channel, the navigation performance in complex tasks cannot be maintained.
3) Comparing `MRV-C` with `MRV-A`, the former one has the higher success rate, whereas the latter one has the lower path length and moving step. This indicates that `MRV-A` has better local coordination performance. In addition, comparing `SRV` with `MRV-C`, we can find that the former one has the slightly lower path length but much smaller success rate (note that we only consider successful cases in path length), which implies that when local motion conflict occurs, `SRV` tends to wait in place, while `MRV-C` has the stronger ability to avoid conflicts by introducing local path detours.

TABLE IV
SCALABILITY RESULTS TO DIFFERENT ROBOT NUMBERS

	Success Rate	Path Length	Moving Step
	Robot Number = 10		
SRV	82.13%(10.93%)	1.90(0.56)	160.88(75.96)
MRV-C $\backslash w.$ *SC*	87.20%(14.70%)	2.31(0.84)	185.57(89.42)
MRV-C	**94.27%(8.11%)**	1.90(0.56)	146.32(76.99)
MRV-A	92.00%(10.77%)	**1.82(0.56)**	**127.66(69.75)**
	Robot Number = 30		
SRV	72.33%(9.55%)	1.91(0.58)	205.77(90.57)
MRV-C $\backslash w.$ *SC*	21.40%(9.81%)	3.09(1.30)	360.91(102.38)
MRV-C	**87.13%(7.34%)**	1.93(0.57)	184.80(87.36)
MRV-A	83.00%(8.93%)	**1.81(0.53)**	**177.17(87.98)**
	Robot Number = 50		
SRV	60.73%(7.63%)	1.92(0.57)	247.36(96.54)
MRV-C $\backslash w.$ *SC*	7.92%(4.27%)	3.14(1.45)	386.09(95.25)
MRV-C	**77.92%(7.84%)**	1.95(0.58)	222.05(94.52)
MRV-A	72.25%(8.27%)	**1.85(0.56)**	**219.55(95.54)**

TABLE V
GENERALIZABILITY RESULTS TO DIFFERENT OBSTACLE DENSITIES

	Success Rate	Path Length	Moving Step
	Obstacle Density = 8%		
SRV	74.20%(14.06%)	1.88(0.54)	197.37(84.51)
MRV-C	**89.67%(9.48%)**	1.90(0.54)	181.24(88.38)
MRV-A	86.13%(12.32%)	**1.81(0.55)**	**159.40(78.99)**
	Obstacle Density = 12%		
SRV	66.67%(15.17%)	1.88(0.58)	231.21(97.44)
MRV-C	82.13%(12.47%)	1.87(0.56)	206.84(91.56)
MRV-A	**82.73%(12.36%)**	**1.83(0.57)**	**185.84(89.73)**

D. Generalizability to Crowded and Large Environments

In this section, we first test different models in the 60 × 60 map with ten robots, and we increase the static obstacle density to 8% and 12%. The results in Table V show that: 1) compared with `SRV`, the success rate degradation of `MRV-C` and `MRV-A` in crowded environments are much lower; 2) `MRV-C` performs better in success rates, while `MRV-A` has the shortest path length and moving step; and 3) comparing Tables IV and V, the path length of all the models remains basically unchanged, but moving step increases with the increase of the static density. This implies that, in the crowded environments, each robot is more likely to wait in place for local motion coordination.

We then test different models in an extremely crowded environment, i.e., the 40 × 40 map with 12% obstacle density and 50 robots (about 25 times crowdedness than the training case). In this environment, the multirobot cooperative navigation task becomes very challenging as each robot should handle frequent motion conflicts and the free space for local motion coordination is also very limited. From the results shown in Fig. 6(a), we can find that our approaches still have a success rate higher than 50%, which is much better than `SRV`. The differences between `MRV-C` and `MRV-A` in both metrics are not obvious. The potential reason is that, since in such an environment the space is very crowded, introducing attention

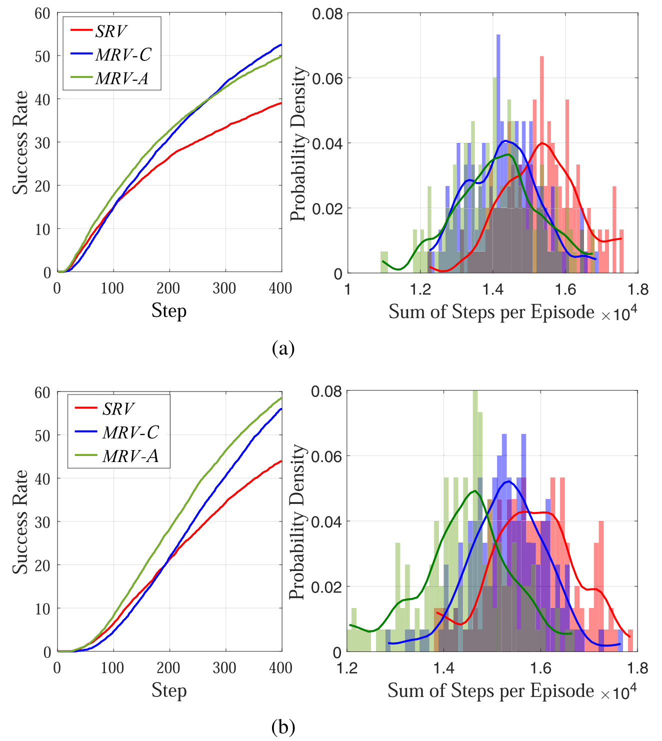

Fig. 6. Generalizability to crowded and large environments. In each test, the left subfigure shows the success rate (proportion of destination-arrived robots) at each step of each model and the right one shows the histogram (density distributions) of the sum of moving steps. (a) Results in the extremely crowded environment. (b) Results in the large environment.

cannot largely improve model ability. In order to verify this claim, we further test different models in a large environment, i.e., the 100 × 100 map with the same 12% obstacle density and 50 robots. The results in Fig. 6(b) show that `MRV-A` outperforms `MRV-C` as there are enough local coordination spaces, and thus, introducing attention will enable each robot to find out a more efficient local path. In addition, the variance of the density distribution of `MRV-C` and `MRV-A` in the large environment is also lower than that in the extremely crowded environment.

E. Interpretation Results

As shown in Fig. 7, we calculate the gradient of original input observations on the final robot actions and visualize the importance (heat value) of each pixel. The results answer the following questions.

1) Which Parts of Each Robot's Own Observation Contribute Most to Its Final Action: As an example, Fig. 7(d) visualizes the contribution of each pixel in the original input of robot 3 to its own final action, which shows that the area corresponded to the goal direction contributes most. In addition, the directions that correspond to the movable paths are also highlighted (note that we only mark directions 1–4 as examples, and other highlighted areas also correspond to movable paths). The above results illustrate that the perception module of each robot has successfully learned the

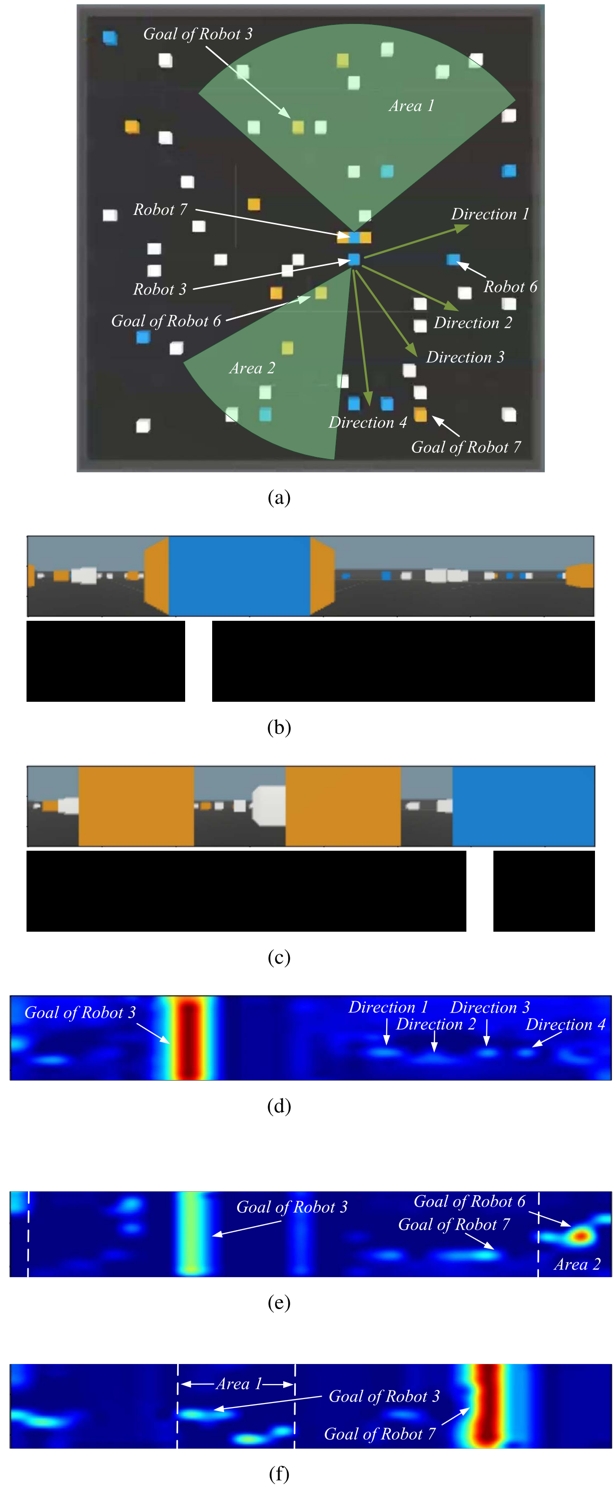

Fig. 7. Interpretation results, where we randomly choose one time step during one test of the trained `MRV-A` model on the 60 × 60 map with ten robots and show the current scenario, real robot input observations, and the visualization results of the action policy interpretation. (a) Bird-eye view of the current scenario. (b) Input observation of robot 3. (c) Input observation of robot 7. (d) Visualization results: the contribution of each pixel in the original input of robot 3 to the final action of robot 3 (red regions have the largest influences, while blue regions contribute the least). (e) Visualization results: the contribution of each part in the original input of robot 3 to the final action of robot 6. (f) Visualization results: the contribution of each part in the original input of robot 7 to the final action of robot 3.

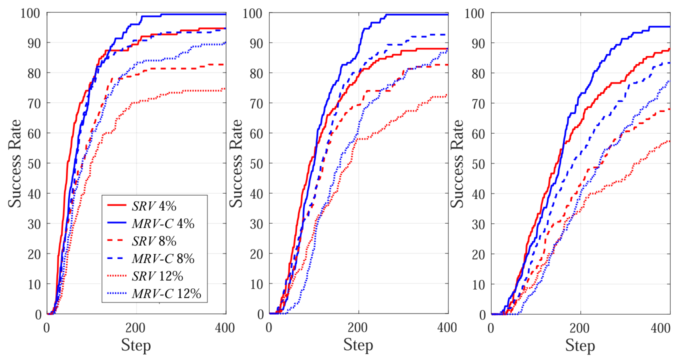

Fig. 8. Singe-robot navigation results. The left, middle, and right figures plot the results of 40 × 40 map, 60 × 60 map, and 100 × 100 map, respectively. In each map, different static obstacle densities, i.e., 4%, 8%, and 12%, are considered.

goal information (main moving direction) and movable area information (obstacle-free directions for potential local motion coordination needs).

2) Which Parts of Neighboring Robots' Input Observations Contribute Most to the Robot's Final Action: We provide two examples here. First, Fig. 7(e) visualizes the contribution of each pixel in the original input of robot 3 to the final action of robot 6. Comparing Fig. 7(d) and (e), we can find that the importance of the area corresponded to the robot 3's goal direction decreases in Fig. 7(e) (but is still highlighted), while the importance of area 2 [as shown in Fig. 7(a)] increases largely, especially the direction corresponded to the goal of robot 6. The above results demonstrate that the GNN module has successfully learned to obtain the information of the interested areas from aggregating other robots' observations. Second, Fig. 7(f) visualizes the contribution of each pixel in the original input of robot 7 to the final action of robot 3. From Fig. 7(a), we can find that robots 3 and 7 should coordinate their local motions as they move to the opposite directions and the local space is very crowded for coordination. Compared with Fig. 7(e), the goal information in Fig. 7(f) is more important as this information is crucial for robot 3 to avoid conflicts with robot 7. In addition, the importance of area 1 [as shown in Fig. 7(a)] is also highlighted, as robot 3 cannot directly see this area (due to view occlusion); however, this area's information is very important for robot 3 to reach its goal. The above results demonstrate that the local coordination feature learning module has successfully learned to aggregate the most important information for local motion coordination and also learned to extend perception range by aggregating other robots' observation features.

F. Single-Robot Navigation

In this section, we test different models in the single-robot visual navigation task to see whether training in the multirobot case will also improve the single-robot navigation performance. As in this case, `MRV-C` and `MRV-A` are exactly the same, so we only compare `SRV` with `MRV-C` for evaluation. As shown in Fig. 8, different map sizes with different obstacle densities are considered and the success rate (proportion of destination-arrived robots) at each step of each model is plotted. The results show that the following conditions hold.

1) Comparing `SRV` and `MRV-C`, we can confirm that training in the multirobot case does improve the single-robot navigation performance, even in this case, there is not any shared messages in the testing. This implies that training in the multirobot case will improve the obstacle-avoidance ability and help robots to handle more complex scenarios. The success rates of `MRV-C` under both the 40 × 40 and 60 × 60 maps with 4% obstacle density are 99.33%, which means that there is only one failure case in the 150 tests.
2) With the increasing map size and obstacle density, the robot needs more moving steps to reach its goal, so the convergence speed of success rate decreases. In addition, the final success rate at the time-out step also decreases as the robot needs to travel a much longer distance while avoiding more obstacles. The results show that the degradation of success rate of `MRV-C` is much lower than `SRV`.

G. Discussion

Based on the above results, we would like to provide a preliminary discussion of the current ability boundary of the IL-based versus RL-based models, and the first-person-view versus bird-eye-view approaches. We choose the state-of-the-art approaches [3], [13] for comparison, which inputs the abstract state observation from the bird-eye view. The IL-based GAT is utilized in [13], while the IL and RL combined approach is used in [3]. As our system input and model framework are totally different from those in [3], [13], we only provide a rough comparison on the success rate.

Li *et al.* [13] said that their models trained with ten robots can maintain the success rate above 92% even as they increase the robot number from 10 to 60 on the 50 × 50 map. In [3], success rate on the 80 × 80 map with 64 robots is higher than 95%. In our experiments, success rate in 60 × 60 map is 95.87% for five robots, 94.27% for ten robots, and 87.13% for 30 robots. The above results show that, in small-scale problems, our model achieves comparable performance with the IL-based approaches with bird-view state inputs. However, we are also noticed that the scalability of our first-person-view RL-based approach is worse than the IL-based approaches with bird-view state inputs, as our success rate drops more quickly in large-scale instances. In our testings, the maximum robot number is set to 50 due to the hardware limitation and the obtained success rate is about 77.92% on the 60 × 60 map; however, in [13], the success rate is above 80% even on the 200 × 200 map with 1000 robots. The results in [3] also show that the success rate is above 80% on the 80 × 80 map with 256 robots. A potential reason is that in the crowded environments with more robots, the raw visual observations are much more complex. As we only train the model with five robots, it is very hard for the perception network to handle the unseen complex observations. In addition, without any expert data, it is more challenging for RL model to learn the motion coordination policy.

VIII. Conclusion and Future Work

In this article, we build the visuomotor learning system for multirobot cooperative navigation using RL. The proposed approach is fully distributed and end-to-end, which can be implemented in unknown environments. Comprehensive results demonstrate the effectiveness, scalability, and generalizability of our models. The obtained results are very promising and move forward a large step to practical applications of multirobot cooperative navigation in industrial and logistic scenarios. Due to hardware limitations, we only test our models with no more than 50 robots in this article, as the raw visual data are much storage and computational costly compared with the state observation data used in the existing works. In the future, we will try to further improve our models' ability in solving large-scale problems with hundreds of robots and also take the domain transfer issue into consideration to conduct physical robotic experiments.

Acknowledgment

The authors would like to thank Binyu Wang and Qingbiao Li for their helpful discussions. They would also like to thank NVIDIA Corporation for their supports of GPUs.

References

[1] Z. Liu, H. Wang, W. Chen, J. Yu, and J. Chen, "An incidental delivery based method for resolving multirobot pairwised transportation problems," *IEEE Trans. Intell. Transp. Syst.*, vol. 17, no. 7, pp. 1852–1866, Jul. 2016.

[2] C. Sun, W. Liu, and L. Dong, "Reinforcement learning with task decomposition for cooperative multiagent systems," *IEEE Trans. Neural Netw. Learn. Syst.*, vol. 32, no. 5, pp. 2054–2065, May 2021.

[3] G. Sartoretti *et al.*, "PRIMAL: Pathfinding via reinforcement and imitation multi-agent learning," *IEEE Robot. Autom. Lett.*, vol. 4, no. 3, pp. 2378–2385, Jul. 2019.

[4] F. Schilling, J. Lecoeur, F. Schiano, and D. Floreano, "Learning vision-based flight in drone swarms by imitation," *IEEE Robot. Autom. Lett.*, vol. 4, no. 4, pp. 4523–4530, Oct. 2019.

[5] Z. Liu, W. Chen, J. Lu, H. Wang, and J. Wang, "Formation control of mobile robots using distributed controller with sampled-data and communication delays," *IEEE Trans. Control Syst. Technol.*, vol. 24, no. 6, pp. 2125–2132, Nov. 2016.

[6] Z. Liu *et al.*, "A synchronization approach for achieving cooperative adaptive cruise control based non-stop intersection passing," in *Proc. IEEE Int. Conf. Robot. Automat. (ICRA)*, May 2020, pp. 236–242.

[7] Z. Liu, W. Chen, H. Wang, Y.-H. Liu, Y. Shen, and X. Fu, "A self-repairing algorithm with optimal repair path for maintaining motion synchronization of mobile robot network," *IEEE Trans. Syst., Man, Cybern. Syst.*, vol. 50, no. 3, pp. 815–828, Mar. 2020.

[8] G. Sharon, R. Stern, A. Felner, and N. R. Sturtevant, "Conflict-based search for optimal multi-agent pathfinding," *Artif. Intell.*, vol. 219, pp. 40–66, Feb. 2015.

[9] J. van de Berg, S. J. Guy, M. Lin, and D. Manocha, "Reciprocal *n*-body collision avoidance," in *Robotics Research*. Berlin, Germany: Springer-Verlag, 2011, pp. 3–19.

[10] Z. Liu, H. Wang, H. Wei, M. Liu, and Y.-H. Liu, "Prediction, planning, and coordination of thousand-warehousing-robot networks with motion and communication uncertainties," *IEEE Trans. Autom. Sci. Eng.*, early access, Aug. 19, 2020, doi: 10.1109/TASE.2020.3015110.

[11] B. Wang, Z. Liu, Q. Li, and A. Prorok, "Mobile robot path planning in dynamic environments through globally guided reinforcement learning," *IEEE Robot. Autom. Lett.*, vol. 5, no. 4, pp. 6932–6939, Oct. 2020.

[12] Z. Liu, B. Chen, H. Zhou, G. Koushik, M. Hebert, and D. Zhao, "MAPPER: Multi-agent path planning with evolutionary reinforcement learning in mixed dynamic environments," in *Proc. IEEE/RSJ Int. Conf. Intell. Robots Syst. (IROS)*, Oct. 2020, pp. 11748–11754.

[13] Q. Li, W. Lin, Z. Liu, and A. Prorok, "Message-aware graph attention networks for large-scale multi-robot path planning," *IEEE Robot. Autom. Lett.*, vol. 6, no. 3, pp. 5533–5540, Jul. 2021.

[14] M. Cap, P. Novak, A. Kleiner, and M. Selecky, "Prioritized planning algorithms for trajectory coordination of multiple mobile robots," *IEEE Trans. Autom. Sci. Eng.*, vol. 12, no. 3, pp. 835–849, Jul. 2015.

[15] R. Tai, J. Wang, and W. Chen, "A prioritized planning algorithm of trajectory coordination based on time windows for multiple AGVs with delay disturbance," *Assem. Autom.*, vol. 39, no. 5, pp. 753–768, Nov. 2019.

[16] V. Digani, L. Sabattini, and C. Secchi, "A probabilistic Eulerian traffic model for the coordination of multiple AGVs in automatic warehouses," *IEEE Robot. Autom. Lett.*, vol. 1, no. 1, pp. 26–32, Jan. 2016.

[17] M. Damani, Z. Luo, E. Wenzel, and G. Sartoretti, "PRIMAL$_2$: Pathfinding via reinforcement and imitation multi-agent learning—Lifelong," *IEEE Robot. Automat. Lett.*, vol. 6, no. 2, pp. 2666–2673, Apr. 2021.

[18] G. Chen *et al.*, "Distributed non-communicating multi-robot collision avoidance via map-based deep reinforcement learning," *Sensors*, vol. 20, no. 17, p. 4836, Aug. 2020.

[19] R. Bonatti, R. Madaan, V. Vineet, S. Scherer, and A. Kapoor, "Learning visuomotor policies for aerial navigation using cross-modal representations," in *Proc. IEEE/RSJ Int. Conf. Intell. Robots Syst. (IROS)*, Oct. 2020, pp. 1637–1644.

[20] F. Zhang, J. Leitner, Z. Ge, M. Milford, and P. Corke, "Adversarial discriminative sim-to-real transfer of visuo-motor policies," *Int. J. Robot. Res.*, vol. 38, nos. 10–11, pp. 1229–1245, Sep. 2019.

[21] P. Mirowski *et al.*, "Learning to navigate in cities without a map," in *Proc. Conf. Neural Inf. Process. Syst.*, 2018, pp. 2424–2435.

[22] W. Gao, D. Hsu, W. S. Lee, S. Shen, and K. Subramanian, "Intention-Net: Integrating planning and deep learning for goal-directed autonomous navigation," in *Proc. 1st Annu. Conf. Robot Learn.*, 2017, pp. 185–194.

[23] Y. Zhu *et al.*, "Target-driven visual navigation in indoor scenes using deep reinforcement learning," in *Proc. IEEE Int. Conf. Robot. Automat.*, May/Jun. 2017, pp. 3357–3364.

[24] A. A. Rusu, M. Večerìk, T. Rothörl, N. Heess, R. Pascanu, and R. Hadsell, "Sim-to-real robot learning from pixels with progressive nets," in *Proc. 1st Annu. Conf. Robot Learn.*, 2017, pp. 262–270.

[25] T.-K. Hu, F. Gama, T. Chen, Z. Wang, A. Ribeiro, and B. M. Sadler, "VGAI: End-to-end learning of vision-based decentralized controllers for robot swarms," in *Proc. IEEE Int. Conf. Acoust., Speech Signal Process. (ICASSP)*, Jun. 2021, pp. 4900–4904.

[26] K. M. Chandy and J. Misra, "Distributed computation on graphs: Shortest path algorithms," *Commun. ACM*, vol. 25, no. 11, pp. 833–837, Nov. 1982.

[27] P. Veličković, G. Cucurull, A. Casanova, A. Romero, P. Lio, and Y. Bengio, "Graph attention networks," 2017, *arXiv:1710.10903*. [Online]. Available: http://arxiv.org/abs/1710.10903

[28] J. Bahamonde, J. Bollen, E. Elejalde, L. Ferres, and B. Poblete, "Power structure in Chilean news media," 2017, *arXiv:1710.06347*. [Online]. Available: http://arxiv.org/abs/1710.06347

[29] A. Juliani *et al.*, "Unity: A general platform for intelligent agents," 2018, *arXiv:1809.02627*. [Online]. Available: http://arxiv.org/abs/1809.02627

Zhe Liu received the Ph.D. degree in control technology and control engineering from Shanghai Jiao Tong University, Shanghai, China, in 2016.

From 2017 to 2020, he was a Post-Doctoral Fellow with the Department of Mechanical and Automation Engineering, The Chinese University of Hong Kong, Hong Kong. He is currently a Research Associate with the Department of Computer Science and Technology, University of Cambridge, Cambridge, U.K. His current research interests include multirobot cooperation and autonomous driving systems.

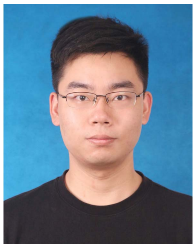

Qiming Liu received the B.Eng. degree in automation from Shanghai Jiao Tong University, Shanghai, China, in 2020, where he is currently pursuing the M.S. degree in control science and engineering.

His current research interests include robot navigation, multiagent coordinated control, and reinforcement learning.

Ling Tang is currently pursuing the bachelor's degree (Hons.) in automation with Shanghai Jiao Tong University, Shanghai, China.

His current research interests include robot navigation and multirobot cooperation.

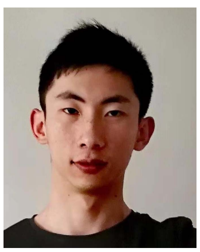

Kefan Jin received the B.Eng. degree in ocean engineering from Harbin Engineering University, Harbin, China, in 2016. He is currently pursuing the Ph.D. degree in ocean engineering with Shanghai Jiao Tong University, Shanghai, China.

His current research interests include multiagent cooperation, unmanned surface vehicle, and autonomous driving systems.

Hongye Wang received the B.S. degree in detection, guidance and control technology from Northwestern Polytechnical University, Xi'an, China, in 2020. He is currently pursuing the master's degree with the Department of Automation, Shanghai Jiao Tong University, Shanghai, China.

His research interests include autonomous mobile robots, multirobot cooperation, and autonomous driving systems.

Ming Liu (Senior Member, IEEE) received the B.A. degree in automation from Tongji University, Shanghai, China, in 2005, and the Ph.D. degree from the Department of Mechanical Engineering and Process Engineering, ETH Zürich, Zürich, Switzerland, in 2013.

He was a Visiting Scholar with Erlangen Nurnberg University, Erlangen, Germany, and the Fraunhofer Institute IISB, Erlangen. He is currently an Assistant Professor with the Department of Electronic and Computer Engineering, The Hong Kong University of Science and Technology, Hong Kong. His current research interests include autonomous mapping, visual navigation, topological mapping, and environment modeling.

Dr. Liu was a recipient of the Best Student Paper Award from IEEE MFI 2012, the Best Paper in Information Award from IEEE ICIA 2013, the Best RoboCup Paper from IEEE IROS 2013, the Best Conference Paper Award from IEEE CYBER 2015, the Best Student Paper Award from IEEE ICAR 2017, and the Best Paper in Automation Award from IEEE ICIA 2017. He received twice the innovation contest Chunhui Cup Winning Award in 2012 and 2013. He received the Wu Weijun AI Award in 2016 and the IROS Toshio Fukuda Young Professional Award in 2018. He serves on the Editorial Board of IEEE ROBOTICS AND AUTOMATION LETTERS.

Hesheng Wang (Senior Member, IEEE) received the B.Eng. degree in electrical engineering from Harbin Institute of Technology, Harbin, China, in 2002, and the M.Phil. and Ph.D. degrees in automation and computer-aided engineering from The Chinese University of Hong Kong, Hong Kong, in 2004 and 2007, respectively.

He is currently a Professor with the Department of Automation, Shanghai Jiao Tong University, Shanghai, China. His current research interests include visual servoing, service robots, computer vision, and autonomous driving.

Dr. Wang was the General Chair of the IEEE RCAR 2016 and the Program Chair of the IEEE ROBIO 2014 and IEEE/ASME AIM 2019. He is the General Chair of IEEE ROBIO 2022. He served as an Associate Editor for the IEEE TRANSACTIONS ON ROBOTICS from 2015 to 2019. He is also an Associate Editor of IEEE TRANSACTIONS ON AUTOMATION SCIENCE AND ENGINEERING, IEEE ROBOTICS AND AUTOMATION LETTERS, *Assembly Automation*, and the *International Journal of Humanoid Robotics*, a Technical Editor of the IEEE/ASME TRANSACTIONS ON MECHATRONICS, and an Editor of the Conference Editorial Board (CEB) of IEEE Robotics and Automation Society.